

LOW GAIN AVALANCHE DETECTORS FOR PROTON-CT

Gregor Kramberger*

Jozef Stefan Institute, Ljubljana, Slovenia

Abstract. With increasing number of hadron therapy centres the need for proton-CT as a powerful imaging technique is growing. Although a number of experimental p-CT has been developed there is no clinical p-CT yet. The imaging technique is based on measuring entry and exit point of the proton from the tissue as well as the residual energy of the proton. The latter is very demanding in terms of high particle rates and required resolution. The p-CT concept using novel Low Gain Avalanche Detectors (LGADs) will be described where three layers of LGAD timing detectors are used to measure the proton track and its energy. The measurement of proton energy which is vital for image reconstruction (density of electrons) is obtained from time-of-flight measurements rather than conventional scintillator-based calorimeter. The first-time resolution measurements with very thin (35 μm) LGADs and GEANT4 simulations of the p-CT performance are presented.

Keywords: proton CT, LGAD, 4D tracking, therapy

PACS: 85.30.De, 29.40.Wk, 29.40.Gx 2000 MSC: 60G35

1. INTRODUCTION

Proton therapy provides better dose distributions in the low to intermediate dose range compared to conventional X-ray (photon) therapy (see Fig. 1) [1, 2]. That leads to improved therapy outcomes for certain types of cancer and less side effects. Uncertainties in patient positioning and beam range as well as internal changes of tumour and patient anatomy could, however, compromise treatment effectiveness. That has triggered numerous efforts to develop and improve treatment planning accuracy and image guidance for proton therapy.

During current treatment planning in proton therapy an X-ray computed tomography (CT) dataset of the patient is acquired and the differences of the X-ray attenuation to that expected in the water (Hounsfield units) are converted to the relative stopping power for protons (RSP, related to electron density along the path). This conversion is one important source for range uncertainties, which are typically estimated on the order of 3–5% of the planned proton range.

If treatment planning X-ray CT is replaced with proton CT (p-CT), where individual proton is tracked during the scan, this would lead to the reduction of the planning uncertainty at lower delivered dose. Pre-treatment p-CT would also provide a method for pre-treatment verification of correct patient setup and RSP distribution as well. Currently p-CT is still in pre-clinical stage of developments at different institutions around the world.

The potential advantages of p-CT for image guidance in the treatment room are several:

- lower dose compared to X-ray cone-beam CT
- absence of artefacts often presents in X-ray CT based reconstructions
- using the same radiation source would allow imaging the patient immediately before treatment in the treatment position
- detection of range errors before treatment in addition to serving as a low-dose alignment technique that could replace cone-beam CT.

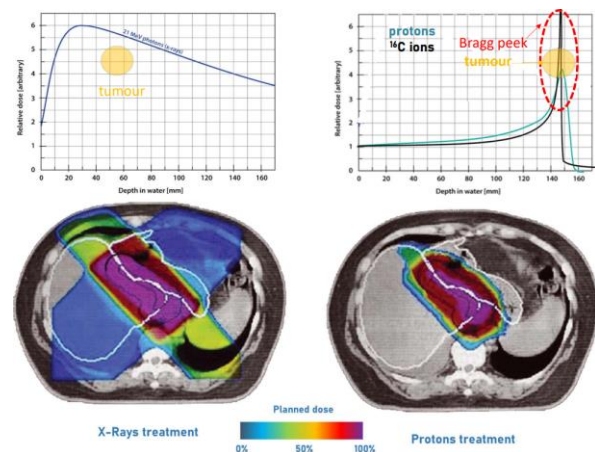


Figure 1. Comparison of photon and hadron based therapy in terms of delivered dose (bottom). Unlike the photons the hadrons deposit most of their energy at the end of the path—Bragg peak in the tumor (top). Adapted from [3].

The information of the drift path and energy from many protons, typically of the order of 100 protons per mm^3 , coming in from many discrete or continuous

* Gregor.Kramberger@ijs.si

directions, is used to reconstruct the distribution of the RSP with sufficient spatial resolution. One of the challenges in proton imaging is the degraded spatial resolution due to multiple Coulomb scattering inside the imaged object. To improve the resolution, several most likely path (MLP) formulations have been proposed and are used in p-CT image reconstruction. Iterative algorithms can then be used to reconstruct 3D p-CT images from radiological projections. With these developments, including fast parallel processing of the acquired p-CT data, a clinical setting for p-CT system appears feasible. Protons can also be used to perform proton radiography, i.e., 2D imaging with protons traversing the patient offering imaging options at the reduced dose.

2. REQUIREMENTS FOR P-CT

Proton computed tomography, i.e., the reconstruction of tomographic images with protons of sufficient energy to penetrate a patient, was originally proposed by A. Cormack [4] and later by Koehler [5] and Hanson et al. [6]. In 2003, a p-CT collaboration was formed with the goal to perform design and simulation studies of pCT and to build a p-CT scanner prototype, based on the measure of the energy loss of the protons [7].

A system was based on conventional particle detectors from high energy physics. Several prototype systems were built in the last decade with a comprehensive review of them given in [8]. Proton CT utilizes position and direction information of the protons before and after the patient and energy deposited by protons while traversing the tumour. The residual energy of the exiting proton is measured in a “calorimeter” as shown in Fig. 2. Most of the prototypes used either Silicon Strip Detectors (SSD), Gas Electron Multipliers (GEM) or Scintillating fibers for tracking and calorimeter based on scintillator detectors (CsI, segmented scintillators). A very complex digital tracking calorimeter with many planes of CMOS sensors measuring the range of protons are also used.

Table 1. Required parameters for a clinical p-CT [9].

Category	Parameter	Value
Proton source	Energy	~ 200 MeV (head) ~ 200 MeV (trunk)
	Energy spread	~ 0.1%
	Beam intensity	$10^6 - 10^9 \text{ p cm}^{-2} \text{ s}^{-1}$
Accuracy	spatial resolution	< 1 mm
	energy resolution	$\sigma_E/E < 1\%$
	electron density resolution	< 1%
Time	instalation time	< 10 min
	DAQ time (10^9 voxels)	< 5 min, up to tens of MHz
	reconstruction	< 15 min (treatment plan) < 5 min (dose verification)
Reliability	radiation hardness	> 1000 Gy
	measurement stability	< 1%
	reconstruction	< 15 min (treatment plan) < 5 min (dose verification)
Safety	max. dose/scan	< 5 cSv
	min. distance to patient	< 10 cm

Although use of these detectors allows for construction of a full scanner, they have many limitations such as sensor-limited acquisition speeds, accurate calibration of calorimeter, its resolution and assembly of different detector technologies.

The p-CT system requirements for successful clinical application of p-CT are listed in Table 1 [9]. The

tracking section of the system is currently mostly realized by position sensitive single sided strip detectors (also gaseous) suitable for covering larger area with smaller number of channels and much easier readout and connectivity with respect to pixel detectors. In order to have space point two such planes are used on each side of the investigated object. The ambiguity in determining the position when multiple protons hit the sensor effectively limits the rate. The required position resolution is moderate by the standards of similar devices used in particle physics and is determined by the voxel size ($\sim 1 \text{ mm}^3$ - limited by scattering) used to reconstruct the path of the proton in the object. Around several 100 p/mm^3 are required to reconstruct the picture with adequate resolution. The acquisition rates for imaging an object of a human head size therefore requires rates of several tens MHz in order to stay within few minutes of examination time mostly with fast pencil scanning proton beams. The precise electron density determination sets the limit of proton’s residual energy to around $\sigma_E/E \sim 1\%$, hence $\sigma_E \lesssim 1 \text{ MeV}$.

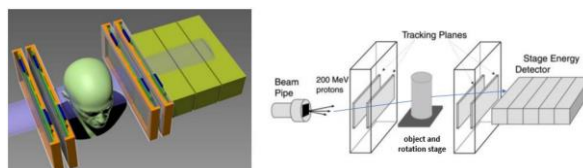


Figure 2. Schematic view of the p-CT system composed of the tracking planes before and after the object and calorimeter. During the p-CT acquisition the object (or system) rotates around the vertical axis (taken from [7]).

There have been many attempts to have a reliable energy resolution, but coupling tracking detectors with calorimeter is a very difficult and leads to large uncertainties. This is also one of the reasons why the development of the p-CT is still in pre-clinical phase.

3. TIME OF FLIGHT P-CT

The energy measurement of exiting protons is possible also by using the time-of-flight providing the time resolution of the sensors and flight paths are appropriate. Recently, novel position sensitive silicon detectors with internal gain, Low Gain Avalanche Detectors - LGAD, have been developed [10, 11]. which allow superb time resolution and good enough position resolution (see section 4). The use of these detectors allows the simplification of the setup shown in Fig. 2 into that shown in Fig. 3.

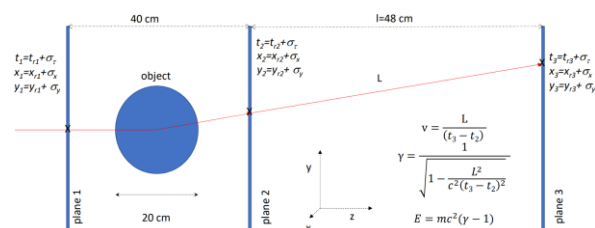


Figure 3. Schematic layout of the proposed system consisting of three planes of LGAD sensors and investigated object – blue sphere.

It consists of minimum 3 planes of pixel detectors which should have sufficient position resolution

(see Table 1). The first two planes (plane1 and plane2) serve as a tracking detector for the impinging protons. The plane2 and plane3 are dedicated to time-of-flight measurement of the proton exiting the investigated object/tumour. As indicated in Fig. 3 the velocity of the exiting proton can be determined from the position and time difference between the hits in the two planes. The energy E_p of the proton is then determined as

$$E_p = m_p c^2 \left[\frac{1}{\sqrt{1 - \frac{(x_3 - x_2)^2 + (y_3 - y_2)^2 + l^2}{c^2 (t_3 - t_2)^2}}} - 1 \right] \quad (1)$$

where c is the speed of light, m_p proton mass and l distance between the planes. It follows from Eq. 1 that the energy resolution depends on the time resolution, i.e. uncertainty of $t_3 - t_2$ measurement. For a sensor time resolution σ_τ the accuracy of the measurement improves with l , but that requires larger instrumented surface. It is therefore crucial to use sensors with superb time resolution. The uncertainty of position resolution has negligible effect on proton energy resolution σ_E as $\sigma_{x,y} \ll l$.

The required energy resolution and achievable time resolution of the sensor planes ($\sigma_\tau \sim 20$ ps) determine the distance between the planes. For the typical energies of the protons exiting the investigated object ~ 100 MeV the distance required for $\sigma_E < 1$ MeV is of order 0.5-1 m which makes construction of such system possible also for clinical use. It is important to stress that unlike for conventional calorimeters, the energy resolution improves at lower proton energies (larger $t_3 - t_2$), therefore allowing adjustment of proton energy to reach optimum performance.

Moreover, the timing information from planes 1 & 2 offers an advantage in more precise determination of the MLP of proton in the investigated object, e.g. by constraining it with the time difference of the hits. Also, location of tissue with more stopping power will influence the time of particle detection in plane 2. At a given energy loss and the hit position there will be a difference in time depending on where the denser tissue is and is indicated in Fig. 4. Therefore, the use of full timing information in calculation of the most likely path and image reconstruction may offer an important advantage over the conventional p-CT design.

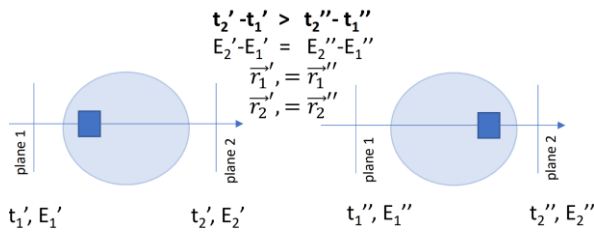


Figure 4. An example of sensitivity of reconstructed proton path to the location of the denser tissue (dark blue box) with larger stopping power. The hit positions and energy loss of the proton is identical in both cases (left/right), but differs in time.

4. LOW GAIN AVALANCHE DETECTORS

Low Gain Avalanche Detectors were developed for track timing in experimental particle physics, most notably for both large experiments ATLAS and CMS built around the upgraded Large Hadron Collider planned for 2029 at CERN [12, 13].

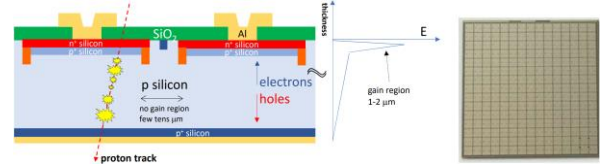


Figure 5. (a) Schematic view of the LGAD detector. The proton track through the sensors is shown with an illustration of the energy deposited along the proton track. (b) Photo of 2x2 cm² LGAD detector with 1.3x1.3 mm² pixels produced as ATLAS prototype [12].

These detectors are similar to conventional silicon pixel or strip detectors ones used in several present p-CT prototypes, but have underneath a highly doped n⁺⁺ layer a highly doped p⁺ layer, 1-2 μm thick, followed by detector bulk (active region) of p-type as shown in Fig. 5). High electric field established between n⁺⁺ and p⁺ layer is responsible for charge multiplication by impact ionization in a similar way as for Avalanche Photo-Diodes (see electric field shape in Fig. 5). The gains of up to ~ 100 were obtained on prototype devices depending on applied voltage, temperature and doping profiles [11]. Such high gain allows for operation of very thin, hence very fast, detectors with ≤ 50 μm thickness, while still retaining excellent signal-to-noise ratio (S/N). These devices are therefore ideal for precise measurement of the time particle/proton crossing the detector with resolutions of O(10 ps).

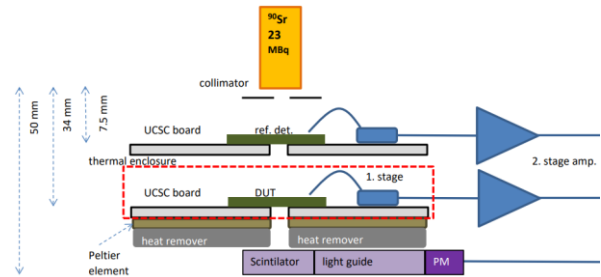


Figure 6. Schematic view of the setup measuring the performance of the prototype sensors - DUT. A fast trans-impedance discrete electronics on UCSC boards is used to readout the signals with a fast-digitizing oscilloscope. The readout is triggered with scintillator coupled to a photomultiplier in coincidence with the reference timing detector (ref. det.).

The sensor time resolution (in combination with electronics) is mainly determined by the time walk and noise jitter (see [11, 14] for details). The latter is roughly determined as $\sigma_{\text{jitter}} \approx t_c / (S/N)$, where t_c is the signal collection time and S/N signal-to-noise ratio. Time-walk and jitter contributions are summed in squares.

The time walk is a consequence of different amount of deposited energy, which is also non-homogeneously distributed along the impinging particle track (see illustration in Fig. 5a for proton track). The induced current in the sensitive electrode has therefore in general different shape and amplitude for every proton. The difference in amplitude can be accounted for/compensated e.g. with measurement of time of crossing the threshold (ToA) and time over that fixed threshold (ToT) or constant fraction discrimination providing that the pulses have same shape. Different shapes of the induced current result in so called non-reducible “Landau time walk” (or “Landau fluctuations”), which dominates the time resolution for

planar detectors with thickness \ll pixel size such as the large pixel LGADs. The achievable time resolution is reduced by the use of thin sensors as spread of the free carrier collection/drift times gets smaller $O(1 \text{ ns})$.

The pixel size of the large $2 \times 2 \text{ cm}^2$ LGAD sensors (see Fig. 5b) developed for HL-LHC applications is $1.3 \times 1.3 \text{ mm}^2$, which means that spatial resolution of $\sigma_{x,y} \sim 375 \mu\text{m}$ can be reached. This is below the required resolution in Table 1. The LGADs are very fast easily achieving the rates needed for clinical use with proper electronics. The current HL-LHC LGAD prototypes have a drawback of not having the 100% fill factor. The field lines in the inter-pixel region don't end in the gain layer (p^+) hence the inter-pixel region is effectively inefficient.

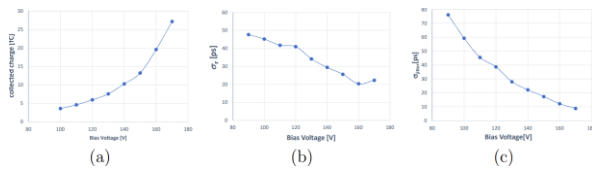


Figure 7. (a) Collected charge dependence on bias voltage for investigated LGAD (b) measured jitter and (c) time resolution of the sensor readout with fast trans-impedance electronics.

The preliminary measurements of the time resolution, jitter and collected charge with detectors suitable for p-CT were measured with the most appropriated prototype sensors produced by Hamamatsu Photonics, Japan (HPK). Their active thickness was $35 \mu\text{m}$ (total device thickness $200 \mu\text{m}$) and a single pixel device was read out with fast electronics. The setup shown in Fig. 6 detects ^{90}Sr electrons. The details about the setup and analysis done can be found in [15].

The measured results at -20°C are shown in Fig. 7. The achievable collected charge reaches almost 30 fC corresponding to gains or around 80. The noise of electronics was around 0.5 fC , hence the measured jitter $\sim 10 \text{ ps}$ was similar to the estimated one. The time resolution of around 20 ps was achieved dominated by Landau fluctuations of around 18 ps . This value is close to the one obtained by simulations [16] and represents the ultimate limit of achievable time resolution with sensors of such thickness. The LGAD detectors are more than sufficiently radiation hard, greatly surpassing the radiation hardness tolerance in Table 1 [12, 13, 14, 15].

5. GEANT-4 SIMULATIONS

The first feasibility studies of the system shown in Fig. 3 were simulated in GEANT4 [17] and shown in Fig. 8. The energy of protons hitting the plane1 perpendicularly was 230 MeV . A water sphere of 20 cm diameter was placed between the plane1 and plane2. The distribution $t_3 - t_2$ is shown in Fig. 9a and largely reflects the time needed for protons to travel the distance between planes 2 & 3. The energy loss in active region of LGADs is shown in Fig. 9b. As can be seen the protons are more ionizing than minimum ionizing particles, in this case around for a factor of five. This fact will should lead to even higher collected charge, hence S/N, than shown in Fig. 9a, but at the same time higher free carrier concentration will lead to larger screening effects [18]. It is therefore important to test the LGADs in the proton beam. According to simulations the

improvement due to smaller Landau fluctuations should be a few ps with respect to the minimum ionizing particles [16].

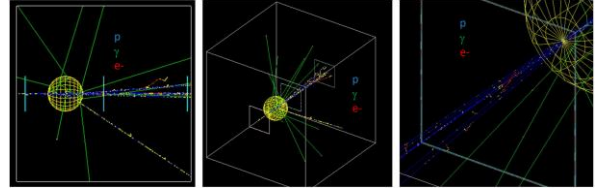


Figure 8. Simulated transport of 230 MeV protons through the water sphere of 20 cm diameter between the three planes of $200 \mu\text{m}$ thick detector ($50 \mu\text{m}$ active thickness and $150 \mu\text{m}$ substrate), $300 \mu\text{m}$ of electronics and 1 mm of PCB. For all three planes the sensor surface is facing towards the beam. The space around the planes is filled with air.

The distribution of the simulated proton energy exiting the plane 2 (MC TRUE) and reconstructed energy using simulated position and ToA in plane 2 & 3 is shown in Fig. 9c. Note the width of MC TRUE distribution due to energy loss fluctuations in the object. The achievable energy resolution is shown in Fig. 9d. The simulated resolution is close to desired one in Table 1 and shows that the time-of-flight approach is feasible. The improvement of the sensor time resolution or larger l lead to improved time resolution. For $l \sim 1 \text{ m}$ the $\sigma_E/E \leq 1\%$ is reached.

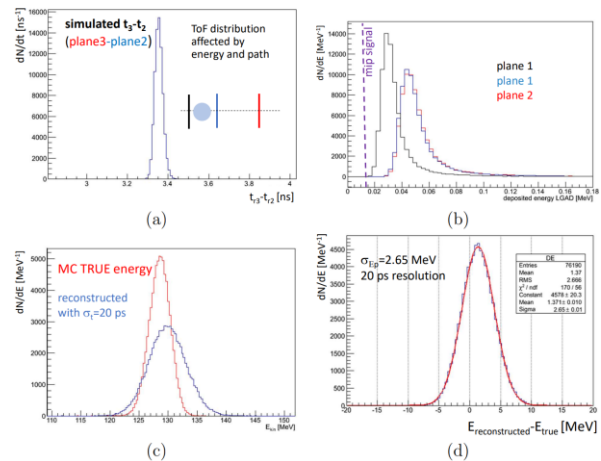


Figure 9. (a) Reconstructed time difference $t_3 - t_2$, (b) deposited energy in active thickness of LGAD for different planes, (c) spectrum of protons leaving plane3 and (d) reconstructed energy resolution.

6. CONCLUSIONS AND OUTLOOK

The construction of p-CT using LGAD sensors seems to be feasible with present state-of-art LGAD sensors. The use of LGADs would greatly simplify the design of the p-CT apparatus by reducing the complexity of several detector technologies and their integration. Moreover, it would offer new approaches in reconstruction, by using timing information from all three layers. The LGADs are radiation hard and can cope with the required particle rates for clinical use. The most challenging and demanding would be the development of application specific electronics (ASIC) tailored to the needs of the p-CT. Presently the readout ASIC for ATLAS-High Granularity Timing Detector [12]

cannot achieve the desired time resolution and also don't have the right functionality. The improvement of jitter contribution and smaller power dissipation are expected by going to more advanced processes, such as [22]. Relatively large pixels however allow lots of the required functionalities to be hosted already by the ASIC thus opening possibilities of simplified post-processing. Although LGADs can be operated at room temperature a fast and complex high-speed electronics would require moderate cooling. It is desired for the system to have low mass for easier reconstruction, hence a lightweight cooling system would be needed. New advances in LGADs try to avoid inefficient gaps between to pixels and lead to better fill factor [19, 20, 21].

Acknowledgements: The author acknowledges the financial support from the Slovenian Research Agency (ARRS J7-4419, ARRS P1-0135).

REFERENCES

- H. Suit et al., "Proton vs carbon ion beams in the definitive radiation treatment of cancer patients," *Radiother. Oncol.*, vol. 95, no. 1, pp. 3 – 22, Apr. 2010. DOI: 10.1016/j.radonc.2010.01.015 PMID: 20185186
- P. Giubilato, "Monolithic Sensors for Proton Therapy," presented at the 10th Int. Workshop on Semiconductor Pixel Detectors for Particles and Imaging (Pixel2022), Santa Fe (NM), USA, Dec. 2022.
- A. M. Cormack, "Representation of a function by its line integrals with some radiological applications," *J. Appl. Phys.*, vol. 34, no. 9, pp. 2722 – 2727, Sep. 1963. DOI: 10.1063/1.1729798
- A. M. Koehler, "Proton radiography," *Science*, vol. 160, no. 3825, pp. 303 – 304, Apr. 1968. DOI: 10.1126/science.160.3825.303 PMID: 17788234
- K. M. Hanson et al., "The application of protons to computed tomography," *IEEE Trans. Nucl. Sci.*, vol. 25, no. 1, pp. 657 – 660, Feb. 1978. DOI: 10.1109/TNS.1978.4329389
- H. F. Sadrozinski et al., "Development of a head scanner for proton CT," *Nucl. Instr. Methods Phys. Res. A*, vol. 699, pp. 205 – 210, Jan. 2013. DOI: 10.1016/j.nima.2012.04.029 PMID: 23264711 PMCID: PMC3524593
- G. Poludniowski, N. M. Allinson, P. M. Evans, "Proton Radiography and Tomography with Application to Proton Therapy," *Br. J. Radiol.*, vol. 88, no. 1053, 20150134, Sep. 2015. DOI: 10.1259/bjr.20150134 PMID: 26043157 PMCID: PMC4743570
- R. W. Schulte et al., "Conceptual design of a proton computed tomography system for applications in proton radiation therapy," *IEEE Trans. Nucl. Sci.*, vol. 51, no. 3, pp. 866 – 872, Jun. 2004. DOI: 10.1109/TNS.2004.829392
- G. Pellegrini et al., "Technology developments and first measurements of Low Gain Avalanche Detectors (LGAD) for high energy physics applications," *Nucl. Instr. Methods Phys. Res. A*, vol. 765, pp. 12 – 16, Nov. 2014. DOI: 10.1016/j.nima.2014.06.008
- H. F. W. Sadrozinski, A. Seiden, N. Cartiglia, "4D tracking with ultra-fast silicon detectors," *ROPP*, vol. 81, no. 2, 026101, Feb. 2018. DOI: 10.1088/1361-6633/aa94d3
- ATLAS Collaboration, *Technical Design Report: A High-Granularity Timing Detector for the ATLAS Phase-II Upgrade*, Rep. ATLAS TDR-031, CERN, Geneva, Switzerland, 2020. Retrieved from: <https://cds.cern.ch/record/2719855> Retrieved on: Sep. 20, 2023
- CMS, Collaboration, *A MIP Timing Detector for the CMS Phase-2 Upgrade*, Rep. CMS-TDR-020, CERN, Geneva, Switzerland, 2019. Retrieved from: <https://cds.cern.ch/record/2667167> Retrieved on: Sep. 20, 2023
- G. Kramberger, "Silicon detectors for precision track timing," presented at the 10th Int. Workshop on Semiconductor Pixel Detectors for Particles and Imaging (Pixel2022), Santa Fe (NM), USA, Dec. 2022. DOI: 10.22323/1.420.0010
- G. Kramberger et al., "Annealing effects on operation of thin Low Gain Avalanche Detectors," *JINST*, vol. 15, no. 8, Po8017, Aug. 2020. DOI: 10.1088/1748-0221/15/08/Po8017
- J. Debevc, "Simulation of Landau fluctuations on timing performance of LGADs," presented at the 42nd RD50 Workshop on Radiation Hard Semiconductor Devices for Very High Luminosity Colliders, Tivat, Montenegro, Jun. 2023.
- S. Agostinelli et al., "Geant4—a simulation toolkit," *Nucl. Instr. Methods Phys. Res. A*, vol. 506, no. 3, pp. 250 – 303, Jul. 2003. DOI: 10.1016/S0168-9002(03)01368-8
- G. Kramberger et al., "Gain dependence on free carrier concentration in LGADs," *Nucl. Instr. Methods Phys. Res. A*, vol. 1046, 167669, Jan. 2023. DOI: 10.1016/j.nima.2022.167669
- G. Paternoster et al., "Trench-Isolated Low Gain Avalanche Diodes (TI-LGADs)," *IEEE Electron Device Lett.*, vol. 41, no. 6, pp. 884 – 887, Jun. 2020. DOI: 10.1109/LED.2020.2991351
- E. Curras et al., "Inverse Low Gain Avalanche Detectors (iLGADs) for precise tracking and timing applications," *Nucl. Instr. Methods Phys. Res. A*, vol. 958, 162545, Apr. 2020. DOI: 10.1016/j.nima.2019.162545
- M. Mandurrino et al., "Demonstration of 200-, 100-, and 50- μ m Pitch Resistive AC-Coupled Silicon Detectors (RSD) With 100% Fill-Factor for 4D Particle Tracking," *IEEE Electron Device Lett.*, vol. 40, no. 11, pp. 1780 – 1783, Nov. 2019. DOI: 10.1109/LED.2019.2943242
- L. Piccolo et al., "The first ASIC prototype of a 28 nm time-space front-end electronics for real-time tracking," presented at the Topical Workshop on Electronics for Particle Physics (TWEPP2019), Santiago de Compostela, Spain, Sep. 2019. DOI: 10.22323/1.370.0022